Biomedical Optics EXPRESS

Digital holographic microscopy of the myelin figure structural dynamics and the effect of thermal gradient

Narges Fathi,[1] Ali-Reza Moradi,[1,2] Mehdi Habibi,[3,4] Daryoosh Vashaee,[5] and Lobat Tayebi[6,7,*]

[1]*Department of Physics, University of Zanjan, PO Box 45195-313, Zanjan, Iran*
[2]*Optics Research Center, Institute for Advanced Studies in Basic Sciences, PO Box 45137-66731, Zanjan, Iran*
[3]*Department of Physics, Institute for Advanced Studies in Basic Sciences, PO Box 45195-1159, Zanjan, Iran*
[4]*Van der Waals-Zeeman Institute, University of Amsterdam, Valckenierstraat 65, 1018 XE Amsterdam, The Netherlands*
[5]*Helmerich Advanced Technology Research Center, School of Electrical and Computer Engineering, Oklahoma State University, OK 74106, USA*
[6]*Helmerich Advanced Technology Research Center, School of Material Science and Engineering, Oklahoma State University, Tulsa, OK 74106, USA*
[7]*School of Chemical Engineering, Oklahoma State University, Stillwater, OK 74078, USA*
**lobat.tayebi@okstate.edu*

Abstract: Myelin figures (MFs) are cylindrical multilamellar lipid tubes that can be found in various healthy and diseased living cells. Their formation and dynamics involve some of the most mysterious configurations that lipid molecules can adopt under certain conditions. They have been studied with different microscopy methods. Due to the frequent coiling of their structure, the usual methods of microscopy fail to give precise quantitative information about their dynamics. In this paper, we introduced Digital Holographic Microscopy (DHM) as a useful method to calculate the precise dynamical volume, thickness, surface and length of the myelin figures. As an example of DHM imaging of myelin figures, their structure and growth rate in the presence and absence of temperature gradient have been studied in this work. We showed that the thickness of a myelin figure can be changed during the first few seconds. However, after approximately ten seconds, the thickness stabilizes and does not alter significantly. We further studied the effect of the thermal gradient on the length growth. The calculation of the length growth from the measurement of the myelin figure volume shows that the length (L) grows in time (t) as $L \propto \sqrt{t}$ at the early stage of the myelin protrusion in both the presence and the absence of the thermal gradient. However, thermal gradient facilitates the growth and increases its rate.

OCIS codes: (090.1995) Digital holography; (090.2880) Holographic interferometry; (120.5050) Phase measurement; (160.1435) Biomaterials; (170.3880) Medical and biological imaging; (180.6900) Three-dimensional microscopy.

References and links

1. D. B. Murphy, and M. W. Davidson, *Fundamentals of Light Microscopy and Electronic Imaging* (Wiley-Blackwell, 2012).
2. D. Gabor, "A new microscopic principle," Nature **161**(4098), 777–778 (1948).
3. U. Schnars and W. Jueptner, *Digital Holography: Digital Hologram Recording, Numerical Reconstruction, and Related Techniques* (Springer, 2004).
4. M. Takeda, H. Ina, and S. Kobayashi, "Fourier-transform method of fringe-pattern analysis for computer-based topography and interferometry," J. Opt. Soc. Am. **72**(1), 156–160 (1982).
5. P. Ferraro, S. Grilli, D. Alfieri, S. De Nicola, A. Finizio, G. Pierattini, B. Javidi, G. Coppola, and V. Striano, "Extended focused image in microscopy by digital holography," Opt. Express **13**(18), 6738–6749 (2005).

#185939 - $15.00 USD Received 26 Feb 2013; revised 11 Apr 2013; accepted 19 Apr 2013; published 24 May 2013

6. B. Javidi, I. Moon, S. Yeom, and E. Carapezza, "Three-dimensional imaging and recognition of microorganism using single-exposure on-line (SEOL) digital holography," Opt. Express **13**(12), 4492–4506 (2005).
7. X. Yu, M. Cross, C. Liu, D. C. Clark, D. T. Haynie, and M. K. Kim, "Measurement of the traction force of biological cells by digital holography," Biomed. Opt. Express **3**(1), 153–159 (2012).
8. M. K. Kim, "Principles and techniques of digital holographic microscopy," SPIE Rev. **1**(1), 018005 (2010).
9. V. Micó, C. Ferreira, Z. Zalevsky, and J. García, "Basic principles and applications of digital holographic microscopy," in *Microscopy: Science Technology, Applications and Education*, A. Méndez-Vilas and J. Díaz, eds. (Formatex Research Center, 2010), pp. 1411–1418.
10. E. Cuche, P. Marquet, and C. Depeursinge, "Simultaneous amplitude-contrast and quantitative phase-contrast microscopy by numerical reconstruction of Fresnel off-axis holograms," Appl. Opt. **38**(34), 6994–7001 (1999).
11. A. Anand, V. K. Chhaniwal, and B. Javidi, "Real-time digital holographic microscopy for phase contrast 3D imaging of dynamic phenomena," J. Disp. Technol. **6**(10), 500–505 (2010).
12. K. Farsad and P. De Camilli, "Mechanisms of membrane deformation," Curr. Opin. Cell Biol. **15**(4), 372–381 (2003).
13. H. Ewers, W. Romer, A. E. Smith, K. Bacia, S. Dmitrieff, W. G. Chai, R. Mancini, J. Kartenbeck, V. Chambon, L. Berland, A. Oppenheim, G. Schwarzmann, T. Feizi, P. Schwille, P. Sens, A. Helenius, and L. Johannes, "GM1 structure determines SV40-induced membrane invagination and infection," Nat. Cell Biol. **12**(1), 11–18 (2010).
14. W. Römer, L. Berland, V. Chambon, K. Gaus, B. Windschiegl, D. Tenza, M. R. E. Aly, V. Fraisier, J. C. Florent, D. Perrais, C. Lamaze, G. Raposo, C. Steinem, P. Sens, P. Bassereau, and L. Johannes, "Shiga toxin induces tubular membrane invaginations for its uptake into cells," Nature **450**(7170), 670–675 (2007).
15. J. C. Stachowiak, C. C. Hayden, and D. Y. Sasaki, "Steric confinement of proteins on lipid membranes can drive curvature and tubulation," Proc. Natl. Acad. Sci. U.S.A. **107**(17), 7781–7786 (2010).
16. D. G. Dervichian, "Swelling and molecular organisation in colloidal electrolytes," Trans. Faraday Soc. **42**, B180–B187 (1946).
17. A. Policard, A. Collet, and S. Pregermain, "Etude au microscope electronique des premiers stades de la lipophanerose dans les cellules histiocytaires," C. R. Hebd. Seances Acad. Sci. **246**, 3405–3407 (1958).
18. W. Stoeckenius, "Oso4-fixierung intrazellularer myelinfiguren," Exp. Cell Res. **13**(2), 410–414 (1957).
19. I. K. Buckley, "Cellular injury in vitro - phase contrast studies on injured cytoplasm," J. Cell Biol. **14**(3), 401–420 (1962).
20. I. K. Buckley, "Microscopic morphology of injured living tissue," Int. Rev. Exp. Pathol. **2**, 241–310 (1963).
21. M. Besisi, *Living Blood Cells and Their Ultrastructure* (Springer-Verlag, 1973).
22. N. Basic-Jukic, M. Coric, P. Kes, L. J. Bubic-Filipi, J. Pasini, and I. Mokos, "Anderson-Fabry disease in kidneys from deceased donor," Am. J. Transplant. **7**(12), 2829–2833 (2007).
23. R. J. Sanderson and A. E. Vatter, "Mode of formation of tubular myelin from lamellar bodies in lung," J. Cell Biol. **74**(3), 1027–1031 (1977).
24. L. M. G. Vangolde, J. J. Batenburg, and B. Robertson, "The pulmonary surfactant system - biochemical aspects and functional-significance," Physiol. Rev. **68**, 374–455 (1988).
25. E. R. Weibel, G. S. Kistler, and G. Tondury, "A stereologic electron microscope study of 'tubular myelin figures' in alveolar fluids of rat lungs," Z. Zellforsch. Mikrosk. Anat. **69**(1), 418–427 (1966).
26. L. N. Zou and S. R. Nagel, "Stability and growth of single myelin figures," Phys. Rev. Lett. **96**(13), 138301 (2006).
27. D. M. Davis and S. Sowinski, "Membrane nanotubes: dynamic long-distance connections between animal cells," Nat. Rev. Mol. Cell Biol. **9**(6), 431–436 (2008).
28. I. Titushkin and M. Cho, "Distinct membrane mechanical properties of human mesenchymal stem cells determined using laser optical tweezers," Biophys. J. **90**(7), 2582–2591 (2006).
29. W. Rawicz, K. C. Olbrich, T. McIntosh, D. Needham, and E. Evans, "Effect of chain length and unsaturation on elasticity of lipid bilayers," Biophys. J. **79**(1), 328–339 (2000).
30. E. Evans and W. Rawicz, "Entropy-driven tension and bending elasticity in condensed-fluid membranes," Phys. Rev. Lett. **64**(17), 2094–2097 (1990).
31. T. J. McIntosh, S. Advani, R. E. Burton, D. V. Zhelev, D. Needham, and S. A. Simon, "Experimental tests for protrusion and undulation pressures in phospholipid-bilayers," Biochemistry **34**(27), 8520–8532 (1995).
32. L. Tayebi, M. Mozafari, D. Vashaee, and A. N. Parikh, "Structural configuration of myelin figures using fluorescence microscopy," Int. J. Photoenergy **2012**, 685617 (2012).
33. I. Tsafrir, M.-A. Guedeau-Boudeville, D. Kandel, and J. Stavans, "Coiling instability of multilamellar membrane tubes with anchored polymers," Phys. Rev. E Stat. Nonlin. Soft Matter Phys. **63**(3), 031603 (2001).
34. I. Sakurai, T. Suzuki, and S. Sakurai, "Cross-sectional view of myelin figures," Biochim. Biophys. Acta **985**(1), 101–105 (1989).
35. C. D. Santangelo and P. Pincus, "Coiling instabilities of multilamellar tubes," Phys. Rev. E Stat. Nonlin. Soft Matter Phys. **66**(6), 061501 (2002).
36. M. Haran, A. Chowdhury, C. Manohar, and J. Bellare, "Myelin growth and coiling," Colloids Surf. A Physicochem. Eng. Asp. **205**(1-2), 21–30 (2002).
37. K. Mishima, T. Ogihara, M. Tomita, and K. Satoh, "Growth rate of myelin figures for phosphatidylcholine and phosphatidylethanolamine," Chem. Phys. Lipids **62**(2), 87–91 (1992).
38. L. N. Zou, "Myelin figures: the buckling and flow of wet soap," Phys. Rev. E Stat. Nonlin. Soft Matter Phys. **79**(6), 061502 (2009).

#185939 - $15.00 USD Received 26 Feb 2013; revised 11 Apr 2013; accepted 19 Apr 2013; published 24 May 2013

1. Introduction

Most of the biological samples are relatively transparent. Since the microscopic techniques can detect only the intensity and color of the light of field-sample interaction, staining methods are used to provide contrast through such samples. The optical phase changes by a transparent sample provide valuable structural information of the samples, and methods such as phase contrast and differential interference contrast microscopy have been utilized to image boundaries of phase objects within the sample [1]. However, these techniques are inherently qualitative. Several attempts have been presented to resolve this problem with more quantitative approaches. Among various techniques, holography has been emphasized and developed more than others [2]. Holography is capable of three dimensional (3D) information recording. Optical reconstruction is also possible via visual 3D observation. Conventional holography suffers from drawbacks such as the need for photographic development of holograms and extra facilities for quantitative 3D analysis. Digital holography can be a solution for these shortcomings. It works based on recording the holograms by digital image sensors followed by their numerical reconstruction [3,4]. Subsequent reconstruction of the hologram contains the information about the phase object. In recent years, extensive research has been dedicated to the expansion of different applications of digital holography [5–7]. A significant advantage of holography is its capability to integrate with conventional microscopes to perform digital holographic microscopy (DHM) [8,9]. DHM provides high resolution quantitative phase contrast imaging that is suitable for non-invasive investigations of living cells and many other industrial life sciences and medicine applications [10,11].

In this paper, for the first time, we utilize DHM technique for myelin figures (MF) imaging. MFs are multilamellar cylindrical tubes of membrane lipids. In living cells, such tubules are generated via a highly regulated transduction of physical forces [12]. Morphologically similar membrane tubules also form when plasma membranes are deformed by binding with bacterial toxins in their extra-cellular space, e.g., shiga and cholera toxins [13–15]. Multilamellar tubules of MFs, are found in healthy and diseased cells as transient and long-lived structures originating from concentrates of dense lipid plaques [16–18]. Case in point of such cells and biological organelles include Histiocyte cell in lung [19,20], aged red blood cell [21], Mesangial cell and Podocytes in kidney [22]. A prominent example is the existence of MFs in pulmonary lining. They have been implicated in the formation of extra-cellular lipid-protein coat at the alveolar surface, whose primary function is to facilitate decrease in the surface tension when lungs deflate [23–25]. These extra-cellular MFs form when intracellular lamellar bodies secreted into the alveolar lumen experience chemical stresses due to changes in pH and ion (e.g., Ca++ and Mg++) concentrations [23,25].

Generally, stacks of lipid amphiphilic molecules in excess water and at the presence of an external stress/force have great capability for the formation of multilamellar cylindrical tubes. For example lamellar bodies in lung convert to multilamellar tubular configuration in response to stress [23]. A dry plaque of lipid would make many MFs after applying the stress caused by hydration. Even the hydrated stack lipids can make MF at the presence of sufficiently strong external flow [26].

Cylindrical tubes also have an important role in long-distance communication between biological cells and in pathologies [27]. They have also been used in studying the physical properties of some amphiphiles such as lipid bilayers by pulling out tethers [28–31].

So far, imaging of MFs was mostly focused on Fluorescence [32] or Phase Contrast microscopy [33] and to a lesser extent on Scanning Electron Microscope (SEM) [34]. To the best of our knowledge, there is no report of using DHM in studying the myelin figure features. Sample preparation is difficult for SEM imaging and it cannot be used for studying the dynamics of myelin figures. When studying the dynamics using Fluorescence or Dark/Bright field microscope, accuracy and focusing problems exist due to the MF movement in all directions as well as their frequent coiling [35]. Also alteration in the volume of the myelin

#185939 - $15.00 USD Received 26 Feb 2013; revised 11 Apr 2013; accepted 19 Apr 2013; published 24 May 2013

figures cannot be measured by these methods. However, DHM can give us the opportunity to quantitatively consider the structure and dynamics of the myelin figures such as precise evolution of volume, thickness and length of MFs in time.

In this paper, we study the growth of myelin figures employing DHM technique at the presence and absence of linear thermal gradient. The results indicate that thickness of a myelin figure does not alter significantly during its growth. However, it may change at the early stage of the protrusion (< 10 sec.) Our work indicates that length of the myelin figure grows as $L \propto \sqrt{t}$ at the absence or presence of thermal gradient (L = length, t = time). However, thermal gradient facilitate and fasten its growth toward the higher temperature region. Our work provides evidence for the growth based on collective diffusion of lipid molecules in hydrophilic solution [36,37].

2. Materials and methods

1-palmitoyl-2-oleoyl-sn-glycero-3-phosphocholine (POPC) was purchased from Avanti polar lipid. The solution of POPC and chloroform was prepared at concentrations of 10 mg/ml and one microliter drop of the solution was placed in the DHM stage. The drop was air dried at room condition and placed in vacuum for 12 hours for complete evaporation of chloroform. Myelin figures were formed upon hydration of the dry drop.

A special chamber was built in order to conduct temperature gradient on the stage. As shown in the inset of Fig. 1, the chamber consists of a heat source, a cooling pipe and channels for water injection. The heat source includes a thin wire which can be heated by applying electric current via a controlled DC power supply. One side of the chamber is connected to a zero degree water tank via a rectangular shaped capillary as a cooling system. Water constantly passes through the capillary so that the temperature in the cold part remains fixed.

A syringe tip connected to an injection pump was used to flow deionized water into the chamber with a rate of 20 ml/h. The chamber is inserted on the stage of the digital holographic microscope.

The DHM setup is based on a Mach–Zehnder interferometer configuration to allow off-axis holography of a transparent sample, as shown schematically in Fig. 1. A white light illumination source (KL1500 compact, Olympus), collecting lens L1, condenser C, microscope objective MO1 (100X, Olympus) and camera (Thorlabs-DCC1545M) were used to build a conventional home-made inverted microscope. The samples were first viewed through this microscope to adjust the best focus before the holography experiments.

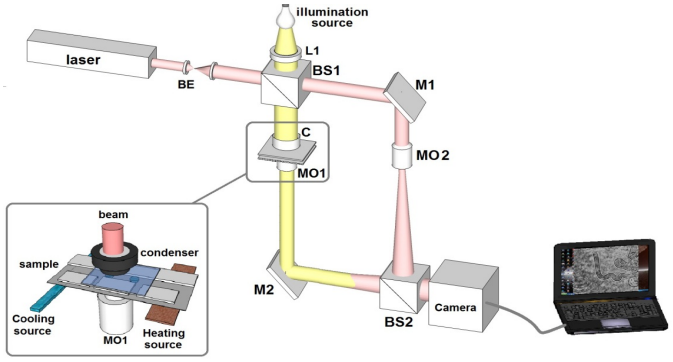

Fig. 1. Schematic DHM setup; M: mirror; BS: beam splitter; MO: microscope objective.

3. Results and discussions

The temperature gradient obtained in our set-up and used in the experiments is shown in Fig. 2(a). Minimum and maximum points correspond to the location of hot and cold sources,

#185939 - $15.00 USD Received 26 Feb 2013; revised 11 Apr 2013; accepted 19 Apr 2013; published 24 May 2013

respectively. Growth of the myelin figures are considered in the direction of cold source to the hot source. The results were compared with the identical room temperature experiment. Figure 2(b) shows a typical image of MFs observed by conventional microscopy. This figure corresponds to t = 10 s after MF formation.

As shown in Fig. 1, laser light emitted from a He-Ne laser (λ = 632.8 nm) after being expanded by beam expander BE is split into object wave and reference wave by beam splitter BS1. Very low laser power ensures that the absorption of laser by the sample and consequent thermal change is negligible. The beam going through mirror M1 is the reference wave, which is sent to camera through MO2 (to adjust the beam curvature) and BS2. The object beam goes through the condenser onto the chamber; and after scattering from the transparent object though MO1, M2, and BS2 goes to the camera to interfere with the reference wave. The interference pattern of the two beams is recorded as a digital hologram and has 3D information of the sample being studied. The recorded holograms will then be reconstructed numerically by computer. The reconstruction process is performed by simulating the diffraction from the digital hologram when illuminated by the reference wave.

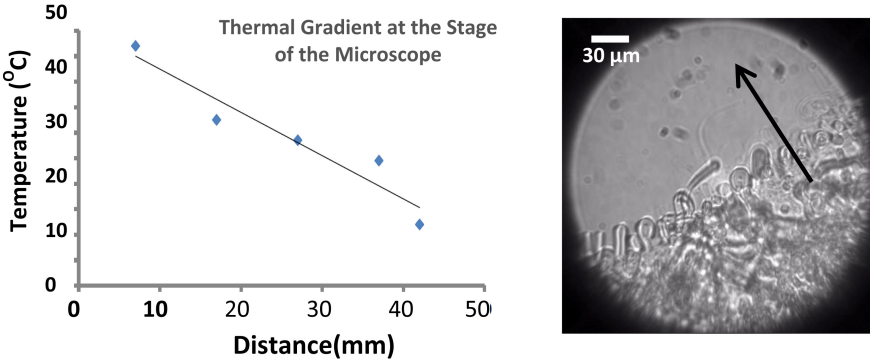

Fig. 2. (a) Temperature gradient used in the experiments; (b) Conventional microscopy image of myelin figures recorded 10 sec. after hydration of the parent lipid dry drop. The arrow indicates the direction of the thermal gradient from low to high temperature. As thermal gradient can act as an external force, it facilitates the growth of MFs.

As shown in Fig. 1, laser light emitted from a He-Ne laser (λ = 632.8 nm) after being expanded by beam expander BE is split into object wave and reference wave by beam splitter BS1. The beam going through mirror M1 is the reference wave, which is sent to camera through MO2 (to adjust the beam curvature) and BS2. The object beam goes through the condenser onto the chamber; and after scattering from the transparent object though MO1, M2, and BS2 goes to the camera to interfere with the reference wave. The interference pattern of the two beams is recorded as a digital hologram and has 3D information of the sample being studied. The recorded holograms will then be reconstructed numerically by computer. The reconstruction process is performed by simulating the diffraction from the digital hologram when illuminated by the reference wave.

We utilized the angular spectrum propagation approach in scalar diffraction theory for numerical reconstruction of the holograms [11]. The propagation can be written as

$$U(x,y,z_0) = FT^{-1}\{U(x,y,0)e^{ik\sqrt{1-\lambda^2 f_x^2-\lambda^2 f_y^2}d}\}, \quad (1)$$

where $U(x,y,0)$ is the complex wavefield of the hologram, f_x and f_y are the spatial frequencies in the x and y directions, respectively, λ is the holography's laser wavelength, and d is the distance of reconstruction plane to the hologram plane. The phase and intensity of the reconstructed wavefront can be computed by

#185939 - $15.00 USD Received 26 Feb 2013; revised 11 Apr 2013; accepted 19 Apr 2013; published 24 May 2013

$$\varphi(x,y)=\tan^{-1}\frac{\mathrm{Im}U(x,y)}{\mathrm{Re}U(x,y)}, I(x,y)=\left|U(x,y)\right|^2, \quad (2)$$

The objects under study in our case are almost transparent and hence we are interested in measurement of phase changes during the experiments. Several holograms were recorded at a rate of 5 frames per second (fps) in various states of MFs growth. Figure 3 shows the reconstruction process and results for a typical hologram of a MF. Figure 3(a) is the recorded hologram of MF at t = 3 s after it started to be formed, and Fig. 3(b) is the Fourier spectrum of the hologram containing two separated images from which one is selected to derive intensity and phase information. Figures 3(c) and 3(d) are the associated phase and intensity patterns of the hologram, respectively. In order to remove the background contaminations from the sample container and the fluid for every sample, we recorded a reference hologram in which no MF is presented. This ensures that the phase changes in various times in MF growth process are only due to its growth. Figure 3(e) is the filtered phase image of the MF subtracted by phase of the reference hologram. Figures 3(f) to 3(h) are different illustrations of the phase information of the reconstruction. Figure 3(f) is the 2D map of a region of interest indicated in Fig. 3(e). As can be seen, the phase of the MF and the rest of the field of view have different value ranges. By a simple RGB to binary transformation of the map, the surface covered by the MF can be calculated. Assuming negligible changes for refractive index, the thickness along an arbitrary line across the MF can also be calculated as shown in Fig. 3(g). 3D map of the phase is shown in Fig. 3(h). The process shown in Fig. 3 should be repeated for all the holograms recorded at a rate of 5 fps for each sample. Changes in thickness, length, surface, or volume of the MF can be used to follow its growth.

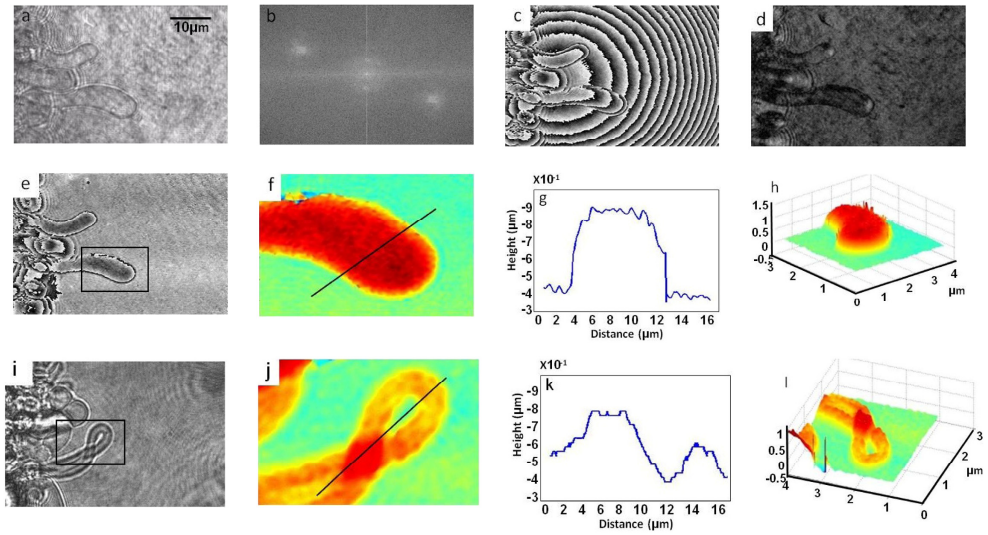

Fig. 3. (a) Hologram of a MF at t = 3 s after its formation starts; (b) Fourier spectrum of the hologram; Associated phase (c) and intensity (d) patterns of the hologram; (e) Filtered phase image of the MF subtracted by phase of the reference hologram; (f) 2D phase map of a cropped part of the reconstructed image; (g) 1D profile of the MF along the line indicated in panel (f); (h) 3D phase map of the MF; (i) to (l): recorded hologram and reconstructed, 1D, 2D and 3D phase map of a coiled MF. Information such as volume, surface, and thickness of the MF can be derived from the reconstruction of holograms. The field of view was 85 µm × 60 µm.

Due to the frequent coiling of myelin figures, studying the dynamic characterization of myelin figure via direct measurement of its length by conventional microscopy can hardly be accurate. Figures 3(i) to 3(l) show a recorded hologram and corresponding reconstructed images of a coiled MF. Coiling is evident from the reconstructed images, showing the

#185939 - $15.00 USD Received 26 Feb 2013; revised 11 Apr 2013; accepted 19 Apr 2013; published 24 May 2013

capability of the DHM method for measurements in such cases. In our DHM technique, we consider the evolution of the volume of the myelin figure in time. Figure 4(a) shows the volume vs. time of a myelin figure at the presence and absence of thermal gradient. Note that the curves indicate the average value of several measurements (more than 20) of various MFs. Red squares show the case in which no temperature gradient is presented, and blue circles show the effect of applying a gradient of temperature in our experiment. Note that the applied temperature gradient is shown in Fig. 2(a) and the direction of MF growth is toward the higher temperature. Figure 4(b), indicates that the thickness of the myelin figure does not change significantly during the growth. However, at the very early stage, in the first ten seconds, more instability is observed in the thickness. In Fig. 4(c), the length of the myelin figure is derived from the values of volume and thickness.

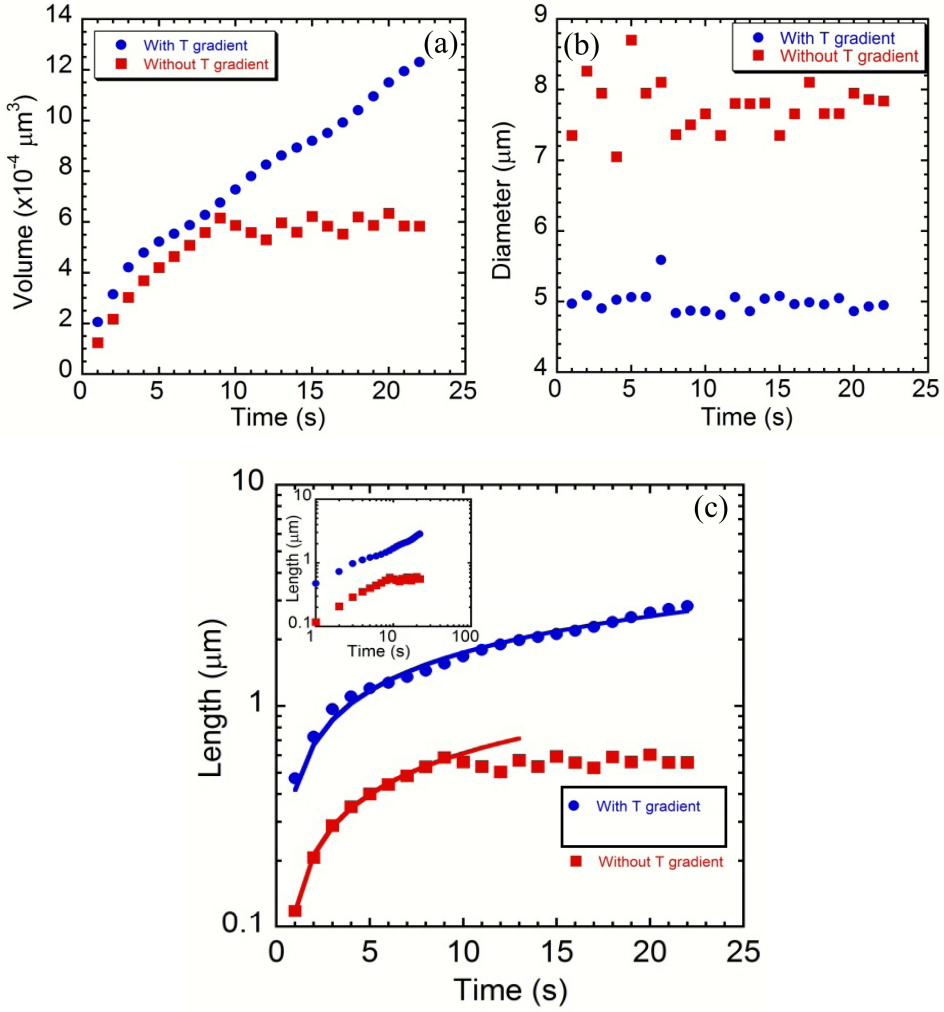

Fig. 4. The effect of temperature gradient on MF growth employing DHM technique. (a) Evolution of volume in time; (b) Thickness of myelin figures does not alter significantly during the growth; (c) Length of myelin figures vs. time at the presence and absence of thermal gradient.

As indicated by the curve fittings, the length of the MF at both presence and absence of the thermal gradient follows the diffusive model of the MF growth [36,37], in which the length evolution is described as .. for the early stage of the growth. Note that, in our

#185939 - $15.00 USD Received 26 Feb 2013; revised 11 Apr 2013; accepted 19 Apr 2013; published 24 May 2013

experiment, the growth of the individual MFs was measured rather than the group of MFs. There are some other reported experiments in which the length of the myelin grows differently (e.g., $L \propto t, or\ L \propto t^{(p)} p \sim 1$) by changing the experimental conditions and the geometry (e.g., applying mechanical puncturing) [26,38]. To the best of our knowledge, the growth of the MFs under thermal gradient has not been studied yet. In this work we showed that applying thermal gradient as a possible external stress does not influence the general length-time relation at the early stage of the growth. However, the thermal gradient increases the rate of the growth, as shown in Fig. 4(c). In this experiment, the MF under thermal gradient grew as $L = 0.61\sqrt{t} - 0.20$ and the MF protruding from similar stacked lipid without thermal gradient grew with about three times slower slope as $L = 0.23\sqrt{t} - 0.11$. Moreover, it was reproducibly observed that MFs under thermal gradient grow for more extended time as $L \propto \sqrt{t}$ and have longer final length.

4. Conclusion

Digital Holographic Microscopy provides a non-destructive and quantitative phase contrast imaging suitable for high resolving investigations of living cells. In this paper, DHM technique was introduced as an accurate technique to study the quantitative dynamics of myelin figures. Specifically, measurements of the volume, thickness and length of the myelin figures, which can hardly be estimated precisely by other microscopy techniques, were presented by DHM method. Our microscope setup was able to provide linear temperature gradients within an acceptable range. After analyzing the results from the numerical reconstruction of the recorded holograms, we discussed the configurational changes and the growth rate at the presence and absence of the thermal gradient.

Acknowledgments

A. R. Moradi acknowledges support of the Center for International Scientific Studies and Collaboration within ICRP program. D. Vashaee acknowledges support of National Science Foundation (NSF) under Grant no. 0933763. N. Fathi acknowledges E. Ahmadi's help for providing with the chemistry lab equipment.

#185939 - $15.00 USD Received 26 Feb 2013; revised 11 Apr 2013; accepted 19 Apr 2013; published 24 May 2013